10.2514/6.2024-2705

Reassessing Jet Mode of Inertial Electrostatic Confinement Thruster for Space Propulsion Application

Rohan Puri*, George H. Miley†, Joshua L. Rovey‡, Myles Y. Gong§ and Erik P. Ziehm¶
University of Illinois Urbana-Champaign, Urbana, Illinois, 61801

Inertial electrostatic confinement (IEC) utilizes strong electric fields to generate and confine plasma. It has been extensively used to conduct nuclear fusion reactions and commercially as a neutron source for activation analysis. This study investigates the two distinct discharge modes, "jet" mode and "spray" mode of an IEC thruster. This paper compares the discharge characteristics of an IEC system for various preliminary design options, such as cathode grid design and cathode grid dimensions. High resolution images are used to conduct intensity analysis at multiple operating points. A basic Faraday probe is used to qualitatively record the change in plasma current density. Results show that biasing the cathode at more negative potentials leads to an increase in current drawn by the grid and the visible intensity of the visible plasma. The current and light intensity increase is gradual until a mode transition from "jet" to "spray" occurs. In other words, the "jet" mode always precedes the "spray" mode. Additionally, background pressure and applied cathode potential are shown to be the two main operating variables for an IEC device. Finally, higher current densities were recorded when the device operated in "spray" mode, however, the ejected plasma was more collimated during "jet" mode.

I. Introduction

A. Background

Inertial Electrostatic Confinement (IEC) is a plasma generation, confinement and extraction technique used primarily for nuclear fusion reactions. Over the years, the applications of an IEC device have increased many-fold due to its ability to create, as well as extract, plasma [1]. Some of those applications include Neutron sources (for Neutron activation analysis), portable X-ray devices, and charged particle accelerators. Lastly, IEC devices are being actively researched as a potential space propulsion system using plasma generated by relatively heavy inert gases as propellant. This study forms the first stage in an attempt to investigate whether the ejected IEC plasma has sufficient momentum per unit weight to propel a space vehicle.

B. IEC Device Structure

In its most basic form, an IEC device consists of a nested electrode structure with the outer one being a solid metal shell and the inner one being a highly transparent grid made of a metal wire. The complete system is kept at a uniform gas pressure much less than that of the atmosphere (usually below 15 mTorr). Keeping the outer shell grounded, a direct current (DC) potential is applied to the inner grid. Plasma is generated in the inter-electrode volume, and the charged particles are confined at the region inside the inner grid. Although various geometries can be used for the nested structure, the two most commonly studied are cylindrical devices and spherical devices [1, 2]. Due to some intrinsic benefits of 3D compression effects in a spherical structure, IEC thrusters were proposed with the spherical design [3, 4]. Additionally, for an ion extraction system (as opposed to an electron extraction one) the smaller grid is applied a negative DC potential, acting as the cathode, while the shell is kept grounded, forming the anode. A graphic of a spherical IEC device is given in Fig. 1.

*Ph.D. Candidate, Aerospace Engineering, University of Illinois Urbana-Champaign, and AIAA Student Member.
†Professor Emeritus, Nuclear, Plasma & Radiological Engineering, University of Illinois Urbana-Champaign, and AIAA Associate Fellow.
‡Professor, Aerospace Engineering, University of Illinois Urbana-Champaign, and AIAA Associate Fellow.
§Undergraduate Research Assistant, Aerospace Engineering, University of Illinois Urbana-Champaign, and AIAA Student Member.
¶Post Doctoral Researcher, Nuclear, Plasma & Radiological Engineering, University of Illinois Urbana-Champaign.

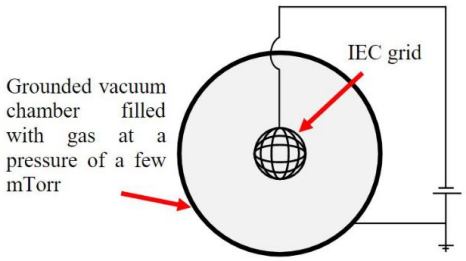

Fig. 1 Schematic of a spherical IEC device [5].

C. Discharge Modes

Depending on the symmetry and the effective transparency of the cathode grid used, an IEC device can operate in three distinct discharge modes - "central-spot" mode, "star" mode, and "halo" mode [6, 7]. A symmetric cathode grid with very small openings (least transparency) is used to achieve the "central-spot" mode. Increasing the transparency in a symmetric grid leads to the "star" discharge mode. Removing the symmetry by enlarging one of the openings in the highly transparent grid leads to the "halo" mode. The "halo" mode is itself divided into two distinct modes - "jet" mode and "spray" mode. Preliminary results indicate that the "jet" mode precedes the "spray" mode, occurrence of both depending on the background gas pressure and voltage applied to the grid. Figure 2 shows all the four discharge modes of an IEC device. It is to be noted that the names of these modes are based on the visual appearance of the visible light emitted by the plasma.

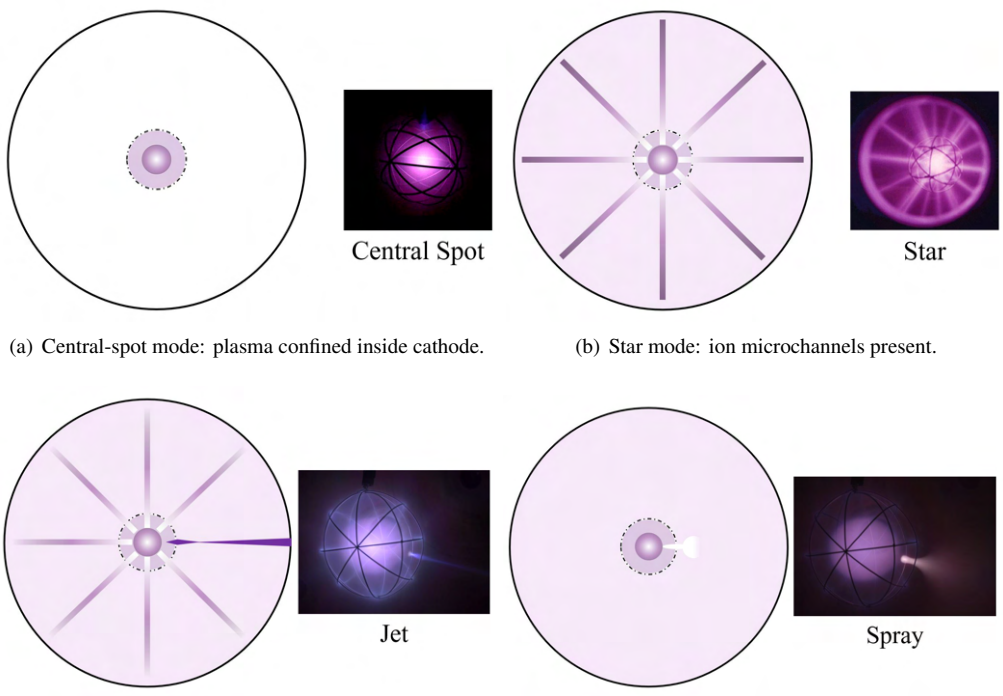

(a) Central-spot mode: plasma confined inside cathode.

(b) Star mode: ion microchannels present.

(c) Jet mode: faint microchannels with one tight beam.

(d) Spray mode: somewhat divergent beam.

Fig. 2 IEC discharge modes - graphic (left) and image (right).

D. Accepted Theories of Operation

The accepted mechanism of IEC is that the plasma generation and confinement is a result of a deep potential well that is formed at the center of the cathode. The ions recirculate between their point of origin (mostly in the inter-electrode

gap), and the point on the equipotential surface diametrically opposite to the origin point. The electric field induced by the cathode causes recirculation of ions, preventing them from hitting the anode walls and in turn raising their energies due to large acceleration [7]. This charged particle movement forms a spherical region inside the cathode with higher probability of ions being present at an arbitrary time, causing an inertial effect that acts as a virtual anode at the center. The virtual anode induces its own electric field, confining electrons between the center and the cathode grid. Thus, the name Inertial Electrostatic Confinement is used to describe such a device. Figure 3(a) describes the charged particle movement inside an IEC system based on the potential well theory. The ion movement in an IEC device operating in "star" mode resemble the spokes of a bicycle wheel, shown in Fig. 2(b). Magnetic deflection tests were done by Miley et al. to confirm the presence of ions in the visible spokes, consequently naming them as ion microchannels [6]. Figure 3(b) shows a SIMION simulation depicting the recirculating ion motion, carried out to confirm the given hypothesis and verify experimental findings [7].

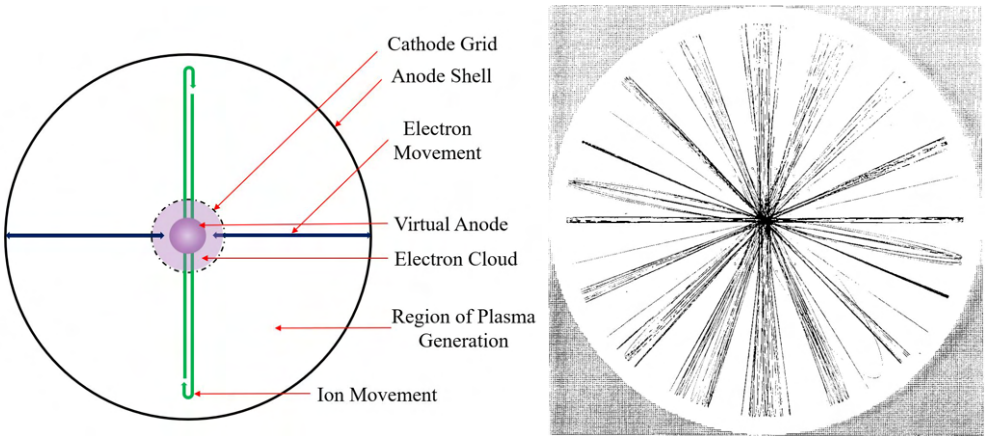

(a) Graphical depiction.

(b) SIMION demonstrating ion recirculation [7].

Fig. 3 Charged particle movement inside an IEC system and the location of the virtual anode.

The above-mentioned potential well theory, along with virtual anode formation, has been indirectly verified by radiation detection experiments for various nuclear (fusion) reactions. Multiple independent numerical and experimental studies of IEC systems, conducted at various universities all over the globe, have acquired results that corroborate the potential well theory. The results of many of these studies have been summarized by Miley and Murali in reference [1]. However, the following unanswered questions, related to the working principle of IEC, have slowed down the progress in this field of study.

- Why doesn't the plasma in the central core get neutralized by ion-electron collisions, leaving high energy neutral atoms in the core?
- Apart from the externally applied electric field, is there an induced electromagnetic field due to charged particle movement that is directly responsible for sustaining the discharge or initiating a mode transition?
- What phenomena is responsible for the occurrence of "jet" mode and "spray" mode?
- Does the plasma beam coming out in the two "halo" modes resemble (visibly as well as with regards to the plasma composition) the ion microchannels observed in "star" mode?
- Is the plasma structure conserved when the background gas is changed from light gases for fusion to heavy inert gases for space propulsion, or when external plasma injection sources are used (such as Helicon in HIIPER [8, 9]).

All of these questions can only be answered once the plasma properties are experimentally measured and their corresponding physics is investigated. Knowing the ion and electron energies, temperature, velocity as well as densities, at various locations inside an IEC system, without disrupting the plasma structure, is the first step in proving any working theory. Following part of this section describes a some additional explanations proposed in an attempt to answer the aforementioned questions.

An alternative plasma structure for the virtual anode was proposed by Farnsworth and Hirsch early on in their research [10]. It described a nested potential wells (virtual electrodes) structure, formed as a result of the movement of ions and electrons inside the cathode. Farnsworth named each consecutive pair of virtual electrodes as a "poissor" (since it represented a solution of the Poisson's equation). However, this approach also does not answer any of the

questions discussed above. Finally, interest in using the IEC with relatively heavier inert gases, as a method of deep space propulsion, started to grow after 2012. Miley's Fusion Studies Lab, at University of Illinois, developed an experimental setup to study "jet" mode with Helicon injected Argon plasma [11]. In parallel, Syring and Herdrich begin investigating the difference between a "jet" mode IEC thruster and a "spray" mode IEC thruster, at the University of Stuttgart, Germany [12]. This resulted in a new theory being proposed, to explain plasma generation and confinement, by Chan and Herdrich. They conducted a momentum balance analysis for "jet"mode operation and concluded that the bright core at the center of the IEC was surrounded by a spherical double layer (SDL) structure, shown in Fig. 4 [13]. This thin SDL creates an electric field on both its sides to attract ions from the central core and electrons from the cathode, forming the distinct boundary of the central core. However, the theory doesn't explain the formation ion microchannels and confinement of high energy ions that undergo fusion. The theory also assumed ion and electron temperatures to be same inside the SDL, which was not experimentally proved or observed by other researchers through direct plasma property measurements. Finally, the questions raised previously were also not addressed by Herdrich et al., and the lack of direct plasma diagnostic results did not give a full understanding of the plasma structure inside the IEC device being studied.

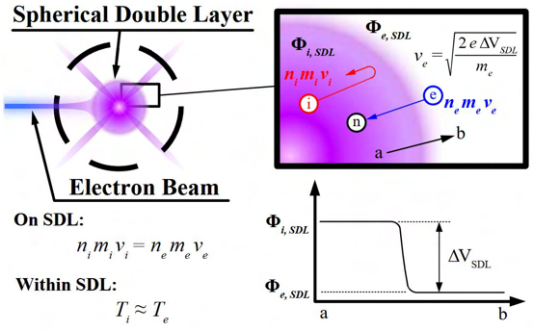

Fig. 4 Spherical double layer structure for the IEC core (claimed virtual anode) [13].

II. Theory of Diagnostics

A. Faraday Probe

A Faraday probe is an electrostatic diagnostic tool that is commonly used to measure ion/electron current density of a given plasma. In basic principles, it consists of a collector electrode that is swept through a range of appropriate DC voltages, and the current collected is recorded at each of those probe potentials. Change in current values with the changing voltages can also be used to identify the source of the current (ions or electrons). Since the focus of this study was not on performance measurement, but to observe and record qualitative changes in the plasma properties of an IEC system, the probe was designed similar to the planar probe with guard ring as described by Mazouffre et al. [14]. The diameter of the planar surface was decided to, additionally, allow Langmuir probe analysis of the recorded IV (current-voltage) characteristics data. Finally, uncertainties due to acquisition devices used was recognised, and accounted for in the results, based on the recommended practices summarized by Brown et al. [15]. Figure 5 shows a representational image of a Faraday probe. For this study, the probe collector was a planar circular surface with an area of 0.04196 cm^{-2} (0.091 inch diameter), surrounded by a circular guard ring of 0.4 inch outer diameter.

Fig. 5 Typical Faraday probe [14].

B. High Resolution Image Analysis

1. Imaging Methods

Due to the complex electric field structure within an IEC system, the structure of the generated plasma is highly complex. Moreover, due to the steep gradient in the brightness of the plasma, dimmer features such as micro-channels are often unnoticeable to the human eye. In order to help build an accurate model of IEC plasma behavior, high resolution images of the plasma were captured at varying pressures and voltages. The objective of this study was to observe trends in the geometry of the plasma in both the core and beam regions. Additionally, metadata from each of the captured images was analyzed to track variations in the intensity of the plasma with changing pressure and voltage.

A Canon EOS Rebel T6 Digital Single-Lens Reflex (DSLR) camera was used to capture RAW images of the plasma. A DSLR camera was chosen for its ability to produce images of high resolution, sharpness and clarity, while offering a large degree of customizability for image settings. In order to accurately reproduce the intensity of the plasma for analysis, careful consideration was made toward the camera settings during data collection. For each experiment, a specific ISO, aperture, and exposure time were selected and maintained throughout the experiment to keep the intensity scale constant. It was also important that the settings be chosen such that the camera would be able to resolve the plasma at low voltages and brightness, while preventing overexposure at higher voltages and brightness. In general, the ISO was maintained at a low values in the range of 100 to 200 in order to improve sharpness, while the aperture was kept as wide as possible to better resolve the image in low-light conditions. Finally, in order to prevent the camera from digitally altering images, manual focus was used and all automatic filters were disabled. During operation of the IEC system, the camera was set on a fixed stand to observe the plasma through a glass viewport in the vacuum chamber. A remote shutter release was used to actuate the shutter without moving or vibrating the camera during experiments.

2. ImageJ Intensity Analysis

The image analysis software, ImageJ, was used to process the high-resolution images collected of the plasma and to create plots of the intensity throughout the image [16]. The intensity scale is based on the particular sensor and settings of the camera used, and is thus not an absolute scale, the relative intensities can be compared across multiple images taken with the same settings. This comparison can be used to identify features in the plasma structure with the highest energy or particle density, as well as how these densities change with varying pressure, voltage, or mode. Figure 6 illustrates the workflow used to create intensity contour plots from the collected images. For each voltage, three images were taken and averaged together in order to further reduce noise and variation. A background subtraction was then applied using a background image taken without the plasma in order to remove any sensor noise. In order to plot the distribution of intensities within each image, each of the processed images were first converted into a 32-bit TIF format. Then, a Lookup Table (LUT) was applied to each image to visually represent intensity variations in a 2D contour plot. The intensity of each pixel is represented as a value ranging from 0 to 255, which was plotted on a scale bar for each image.

Fig. 6 Process for image intensity analysis in ImageJ.

III. Experimental Setup

Experiments for this study are conducted in a 61 cm inner diameter, stainless-steel, spherical vacuum chamber. The vacuum chamber is kept grounded and acts as the anode for the IEC system. A spherical cathode grid is suspended inside the anode shell through a high-voltage feed-through connected to a 15 kV (600 W) DC power supply. Base pressure of 0.05 mTorr is achieved using the combination of a turbo-molecular pump and oil-sealed rotary vane pump.

A 1-10 sccm mass flow controller is used to inject Argon gas inside the chamber, allowing the Argon gas pressure inside to be between 0.5 mTorr and 11 mTorr. Various pressure gauges at multiple locations are used to monitor the pressure inside the system, and a hot-filament ion gauge (±15% accuracy) is used to record the pressure while taking any measurement. Figure 7(a) depicts the general schematic and Fig. 7(b) shows the experimental setup of the IEC research lab where the study was conducted.

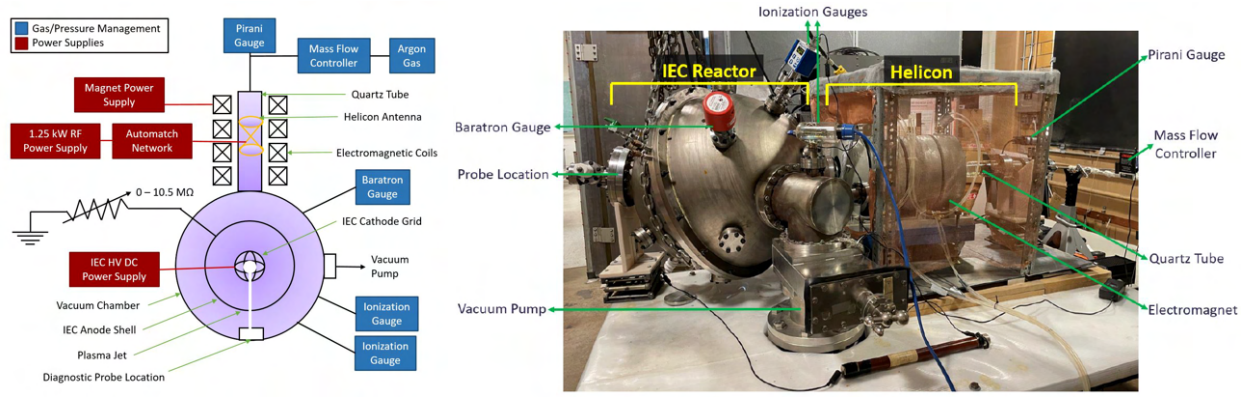

(a) Basic schematic of IEC system.

(b) IEC system at the University of Illinois Urbana-Champaign.

Fig. 7 Experimental setup at the University of Illinois [8].

A. Grid Design

Traditionally, the cathode grids for IEC systems are assembled based on one of the following three designs - Geodesic design (Fig. 8(a)), Globe design (Fig. 8(b)), and Orthogonal design (Fig. 8(c)). The geodesic design comprises of triangular openings (holes) formed by welding rings of equal circumference with equal angle between any two consecutive rings. On the other hand, the globe design consists of grid with wires that form longitudes and latitudes, similar to the ones on Earth, having both triangular and trapezoidal openings (holes). Finally, the orthogonal design uses only three rings of equal circumference, connected such that each individual ring is mutually perpendicular to the other two. Figure 8 shows the three types of spherical grid patterns as described above.

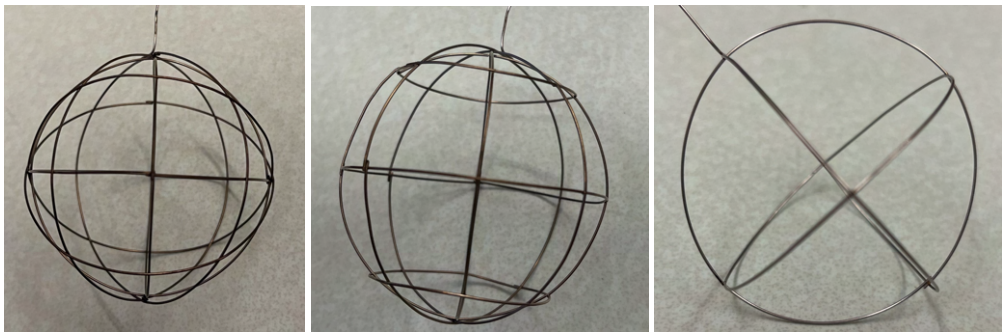

(a) Geodesic design.

(b) Globe design.

(c) Orthogonal design.

Fig. 8 Spherical grid patterns.

A thorough literature survey showed that different research groups have used different designs interchangeably, based on their available manufacturing capabilities. However, direct studies comparing the effect of grid design on the plasma characteristics is still missing from the literature. Preliminary computational studies as well as intuitive understanding indicates a difference in electric field structure induced by each of these grid designs. It is thus expected that a difference in measured properties will be observed, and grid design might be a factor while optimizing IEC systems used for different applications. For this study, preliminary investigation involved recording the discharge characteristics for 5 cm

diameter grids of geodesic as well as globe design. Additionally, two more grids of geodesic design, 10 cm in diameter, were manufactured with difference in the size of the asymmetric opening. It can be seen in Fig. 9 that one of the 10 cm grids looks fairly symmetric compared to the other one, however, both have one opening greater than all the others in the same grid to allow "halo" mode operation. All grids were manufactured using Nickel wire ranging between 0.02 inch and 0.041 inch diameter.

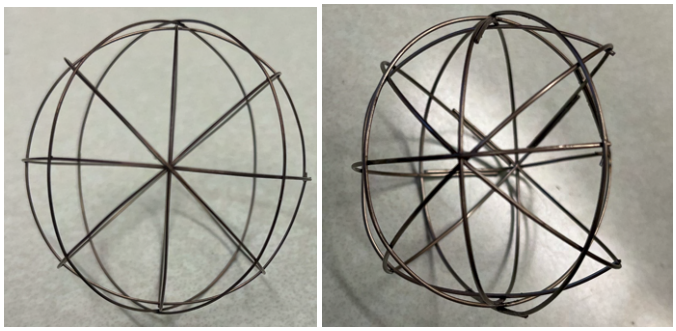

(a) Geodesic grid: minor asymmetry. (b) Geodesic grid: widened asymmetry.

Fig. 9 Geodesic grids with different size of the largest opening.

B. Diagnostics Setup

A Faraday probe was placed right outside the anode to measure the current density of the bulk plasma (not in the beam or ion microchannel path), with changing grid design and/or applied cathode potential. An attempt was made to place two additional Faraday probes, one in the path of the ion microchannel and one directly facing the plasma beam in "halo" mode. However, due to the unknown nature of the "jet"/"spray" and high current recorded in the ion microchannel, the probes were disrupting the steady state operation and interfering with the discharge physics of the device. Hence, this study was carried out by only measuring the current density of the bulk plasma. Additionally, a high resolution camera was used to take pictures of the plasma core and the "jet"/"spray" in order to conduct light intensity analysis of the visual plasma. The camera had fixed exposure settings to allow direct comparison between pictures taken at different points of operation. Figure 10 shows the location of the camera and probe in a schematic of the experimental setup.

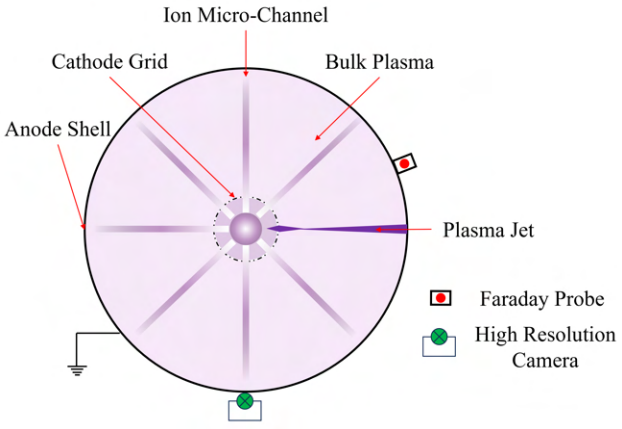

Fig. 10 Diagnostic instrumentation placement.

IV. Results

This section describes the discharge characteristics and visible plasma structure observed when operating an IEC device. Multiple grids were used to observe the effects of grid design and dimension on the plasma behavior. Table 1 lists the grid descriptions of all the grids used in this study.

Table 1 Grid description.

Grid Number	Anode Diameter (cm)	Cathode Diameter (cm)	Design	Average Opening Area (cm^2)	Largest Opening Area (cm^2)	Grid Wire Material	Wire Diameter (cm)
Grid 1	61.0	5.0	Geodesic	3.0	4.0	Nickel	0.051
Grid 2	61.0	5.0	Globe	4.0	4.4	Nickel	0.051
Grid 3	61.0	10.0	Geodesic	7.9	10.5	Nickel	0.100
Grid 4	61.0	10.0	Geodesic	7.9	42.0	Nickel	0.100
Grid C1 [17]	30.0	10.0	Globe	N/A	N/A	Stainless Steel	0.100
Grid C2a [17, 18]	15.0	5.0	Globe	N/A	N/A	Stainless Steel	0.100

A. Paschen Breakdown Point

Paschen curves show the gas breakdown characteristics for a DC plasma system. For the IEC system studied, with the various grid dimensions listed in Table 1, it was observed that the operational discharge region of the device is on the left side of the Paschen curve. Figure 11 shows the Paschen curve plotted for the grids used in this study, alongside a comparison to the breakdown points noted by Herdrich et al. at the University of Stuttgart [17, 18]. It can be seen that the plots for different grids, although fairly close, do not overlap. Additionally, the data from this study did not match the data by Herdrich et al.

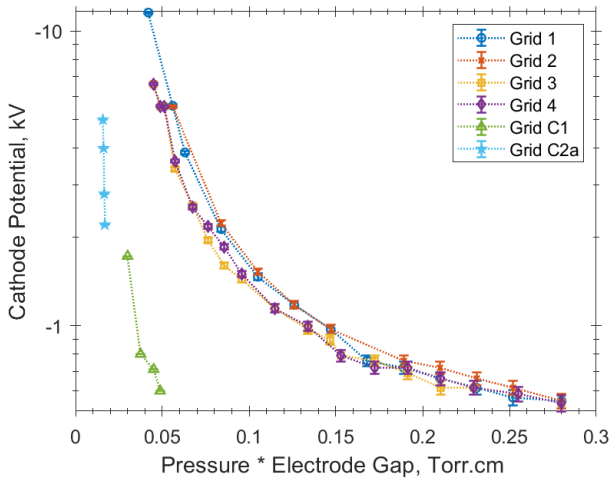

Fig. 11 Paschen breakdown curves.

The breakdown voltage was also plotted as a function of background gas pressure, rather than the pressure × electrode gap distance. Figure 12 shows these results. It can be seen that the points closely overlap in this case and are consistent compared to the recorded values of different experimental setups. This may indicate that the breakdown phenomenon inside an IEC system is dependent on the background pressure alone, rather than the relative spacing between the cathode and the anode.

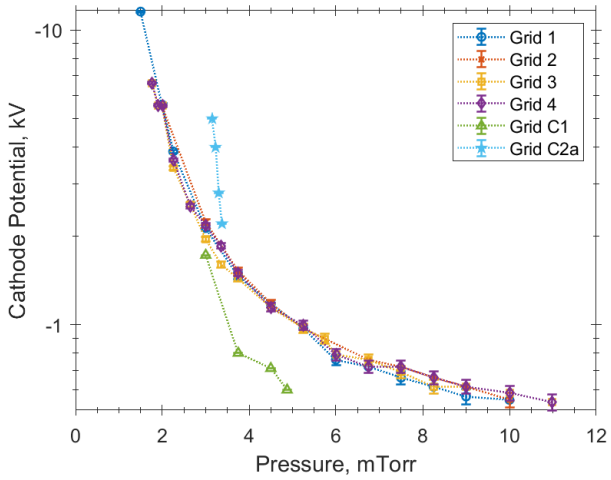

Fig. 12 Breakdown potential as a function of background gas pressure.

B. Grid Design

The current section describes the change in discharge characteristics and observed plasma structure between a geodesic grid and a globe grid, both 5 cm in diameter. Due to excessive grid heating in "spray" mode, grid 1 and grid 2 comparison results primarily focus on the "jet" mode.

1. Discharge Characteristics

The discharge characteristics for grid 1 and grid 2 are shown in Fig. 13. For both the grids, the current increases with the higher values of negative cathode potential, until the grid overheats or a near vertical current jump is observed at which the power supply reaches its current limit. It is also noted that the discharge current is higher for operation at higher background gas pressure. Overall, the currents recorded for "jet" mode operation with both the grids, at same background pressure and cathode potential, are identical.

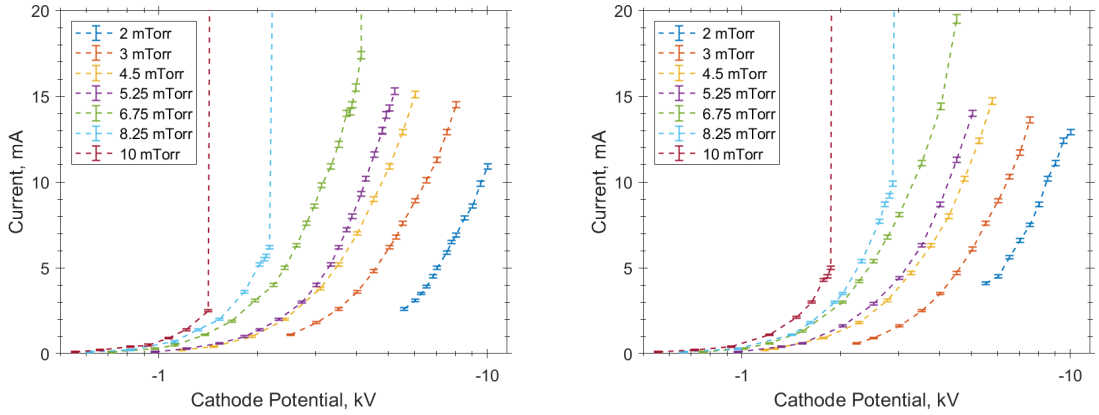

(a) Grid 1: geodesic design.

(b) Grid 2: globe design.

Fig. 13 Discharge characteristics for grid 1 and grid 2.

A difference in discharge characteristics observed between the two grid designs can be seen for the abrupt increase in current. This is observed for background gas pressure equal to or greater than 6.75 mTorr in Fig.13(a) and for pressure greater than or equal to 8.25 mTorr in Fig. 13(b). Comparing the cathode potential values for the points right before this

abrupt current increase, the globe grid has a higher negative cathode potential and discharge current with respect to the corresponding potential and current recorded for geodesic grid.

2. Intensity Analysis

The light intensity analysis to compare grid designs shows two interesting results. By comparing Fig. 14(a) with Fig. 14(c), it is clearly seen that the size of the inner core, shown in the red intensity hotspot, is larger in the geodesic grid for the same background pressure and applied cathode potential. Secondly, comparing Fig. 14(b) and Fig. 14(d), it is also be seen that the inter-electrode region is brighter for the globe grid, compared to the geodesic grid, at the same operating conditions. Lastly, it is noted that the core (high light intensity hotspot in the center of the cathode) formed is more spherical when operating with the globe grid, as opposed to the elongated oval structure observed with the geodesic grid.

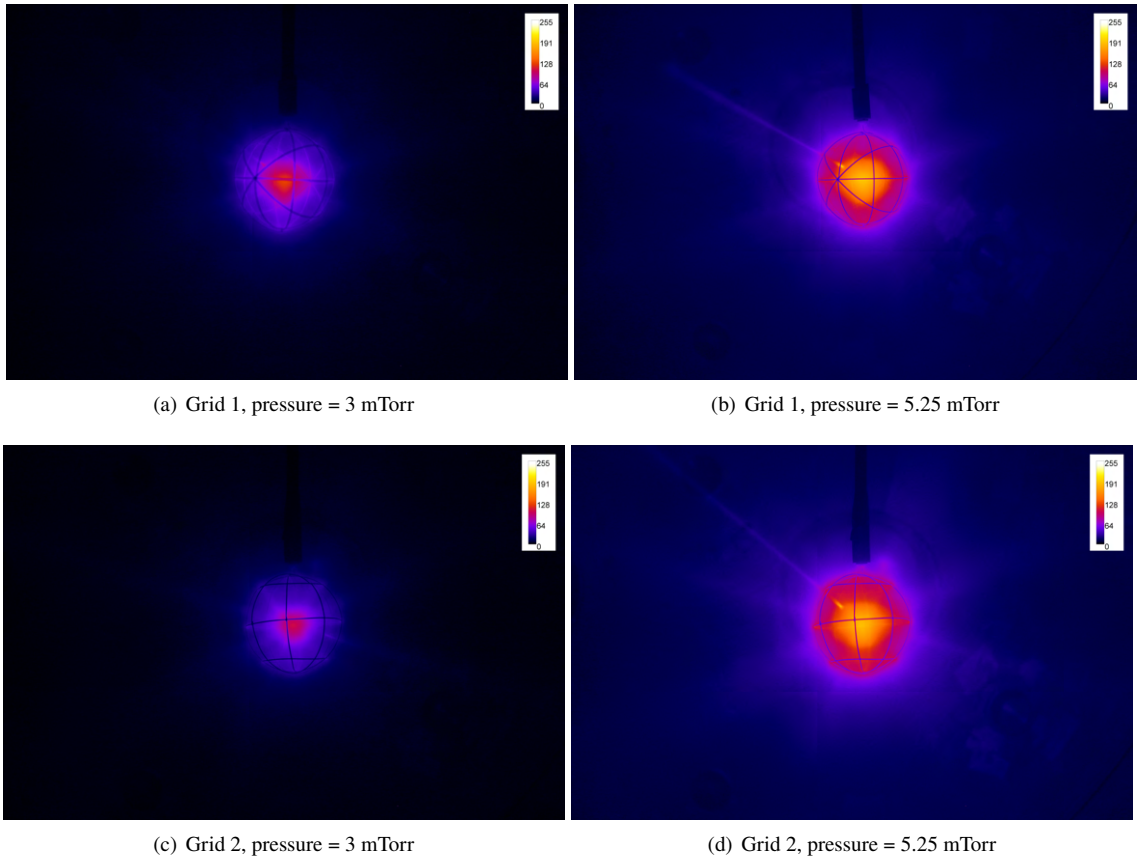

(a) Grid 1, pressure = 3 mTorr

(b) Grid 1, pressure = 5.25 mTorr

(c) Grid 2, pressure = 3 mTorr

(d) Grid 2, pressure = 5.25 mTorr

Fig. 14 IEC operating at cathode potential = -5 kV .

Figure 15 depicts the light intensity distribution at a background pressure where both the grids had the abrupt current increase in the discharge characteristics. The images were captured at the cathode potentials right before the current jump and immediately after the current jump. It was observed that for both the grids, the size of the core remained same before and after the abrupt increase in current. However, the overall light intensity went up significantly. Furthermore in Fig. 15(b) and Fig. 15(d), the structure of the beam coming out of the cathode was more diffuse and curved, as opposed to the beam structure observed in Fig. 15(a) and Fig. 15(c). Lastly, the number of light intensity gradients (similar to distinct boundaries) between various regions inside the device are higher in Fig. 15(b) and Fig. 15(d).

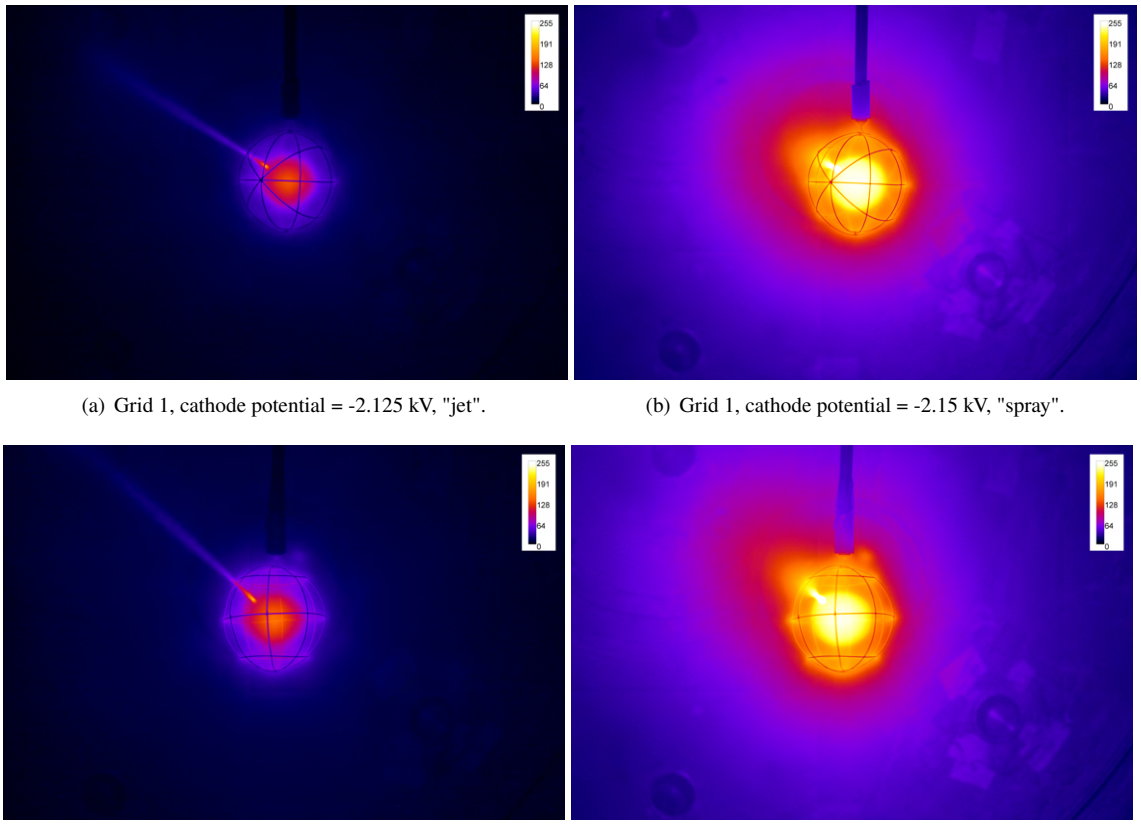

(a) Grid 1, cathode potential = -2.125 kV, "jet".

(b) Grid 1, cathode potential = -2.15 kV, "spray".

(c) Grid 2, cathode potential = -2.435 kV, "jet".

(d) Grid 2, cathode potential = -2.45 kV, "spray".

Fig. 15 IEC operating at background gas pressure = 9 mTorr.

C. Grid Diameter

This section describes the changes observed when varying the diameter of the IEC grids. Two geodesic grids, of diameter 5 cm and 10 cm, are analyzed. The corresponding discharge characteristics and light intensity analysis is presented.

1. Discharge Characteristics

Discharge characteristics for grid 1 and grid 3 are shown in Fig. 16. The current measured for both the grids increased on raising the negative cathode potential. The current values observed for the larger diameter grid were almost double compared to the current values for the smaller diameter grid, at same background pressure and cathode potential. Secondly, grid 1 maintained the gradual increase in current for a larger range of background gas pressures, before encountering the abrupt current increase to power supply limit. This can be observed by the almost vertical current increase in both Fig. 16(a) and Fig. 16(b). For the larger grid, the abrupt current increase happens at the background pressures greater than or equal to 3.35 mTorr. Whereas, the abrupt current increase for the smaller grid happens at background pressures greater than or equal to 6.75 mTorr. Adding to that, the near vertical current increase for the larger grid happens at the cathode potential equal to nearly a third of the corresponding cathode potential for smaller grid, for the same background gas pressure.

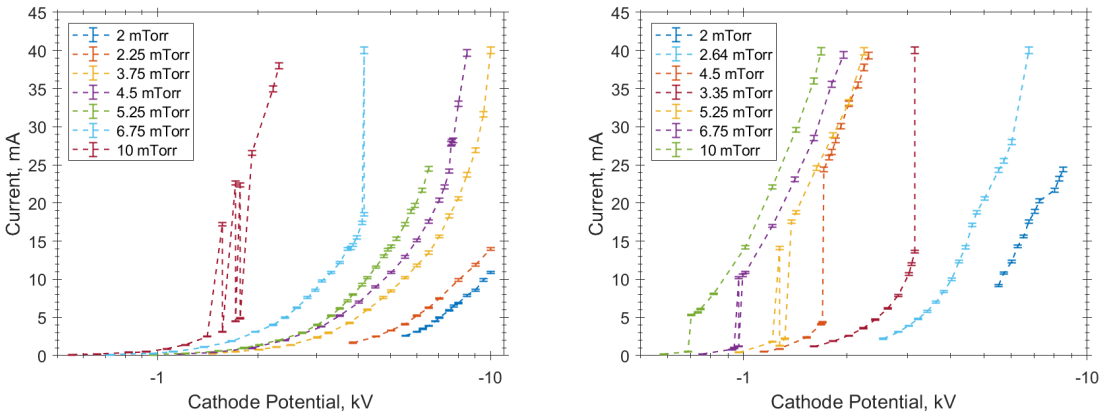

(a) Grid 1: diameter = 5 cm.

(b) Grid 3: diameter = 10 cm.

Fig. 16 Discharge characteristics for grid 1 and grid 3.

2. Intensity Analysis

Images of light intensity analysis for grid 1 and grid 3 operating at background gas pressure of 2 mTorr is given in Fig. 17. Comparing Fig. 17(a) with Fig. 17(c), and Fig. 17(b) with Fig. 17(d), it can be seen that the visible plasma structure is almost identical, but scaled.

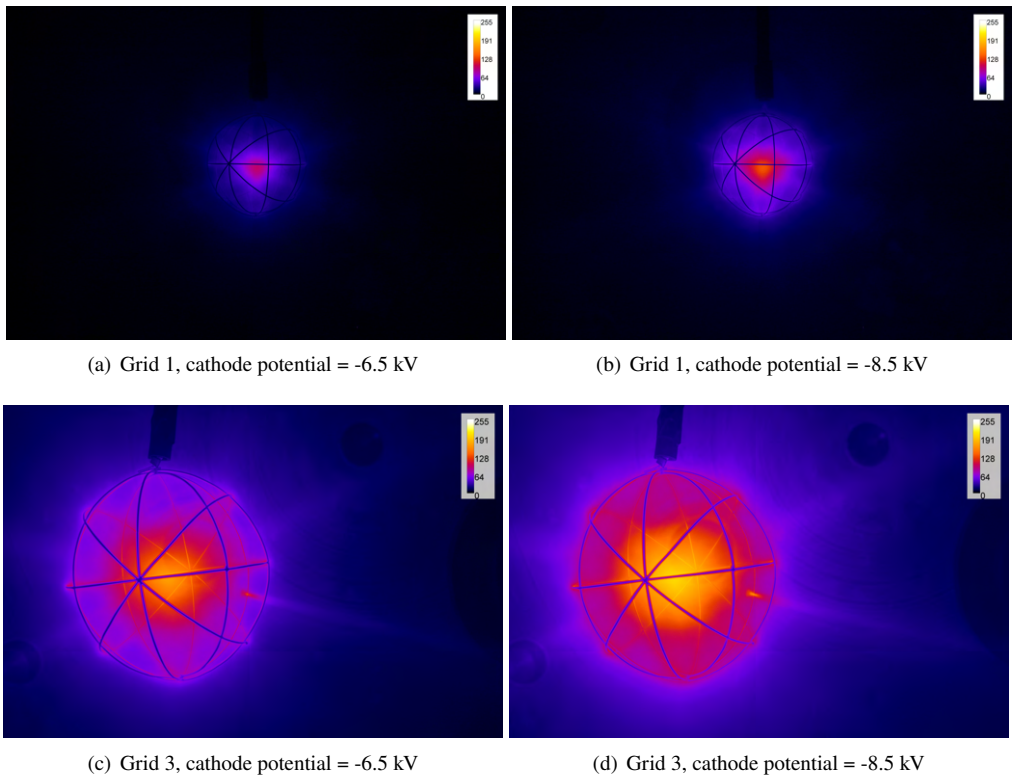

(a) Grid 1, cathode potential = -6.5 kV

(b) Grid 1, cathode potential = -8.5 kV

(c) Grid 3, cathode potential = -6.5 kV

(d) Grid 3, cathode potential = -8.5 kV

Fig. 17 IEC operating at background gas pressure = 2 mTorr.

It is also observed in Fig. 17 that for the smaller grid, the light intensity of the plasma beam is almost comparable to the intensity of the ion microchannels. This makes it harder to notice the beam at lower values of negative cathode

potential. However, for the larger grid the light intensity of the main beam is much more higher and collimated, as opposed to the overall lower light intensity and diffused structure of the ion microchannels. Lastly, the overall brightness is higher for the bigger grid when compared to the smaller grid operating at the same background gas pressure and cathode potential.

Figure 18 show the pictures taken at 6.75 mTorr background gas pressure, at which the abrupt current increase was observed in both the grids. Figure 18(a) and Fig. 18(c) are captured at the cathode potential right before the near vertical current increase as shown in the discharge characteristics. Similarly, Fig. 18(b) and Fig. 18(d) are taken immediately after the abrupt current increase. These images show a drastic change in the light intensity observed before and after the abrupt increase in current is recorded. Additionally, the structure of the beam after the current jump is more curved and less collimated, for both grid 1 and grid 3. Lastly, the light intensity when operating with grid 1, at conditions described in Fig. 18(a) and Fig. 18(b), is considerably higher when compared to that recorded when operating with grid 3, at conditions described in Fig. 18(c) and Fig. 18(d).

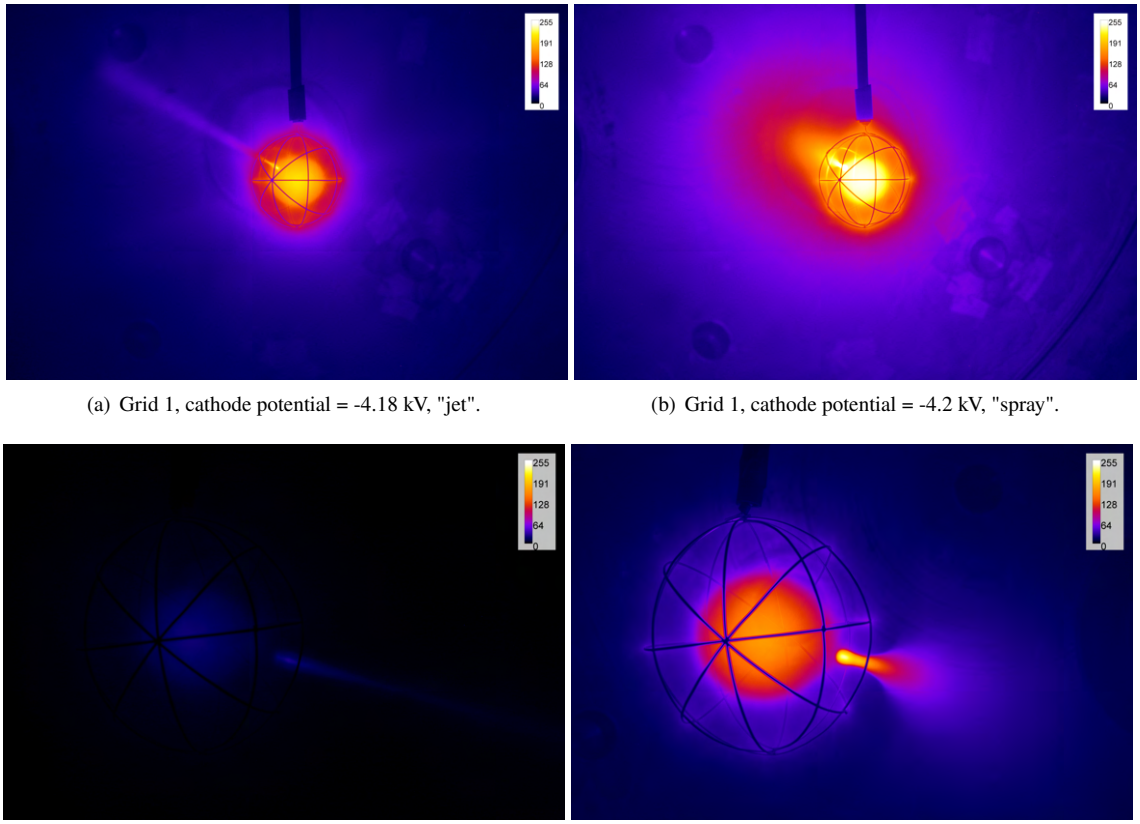

(a) Grid 1, cathode potential = -4.18 kV, "jet".

(b) Grid 1, cathode potential = -4.2 kV, "spray".

(c) Grid 3, cathode potential = -0.98 kV, "jet".

(d) Grid 3, cathode potential = -1.02 kV, "spray".

Fig. 18 IEC operating at background gas pressure = 6.75 mTorr.

D. Background Gas Pressure

The current section presents the results obtained when using background gas pressure as a variable, keeping other operating conditions the same.

1. Discharge Characteristics

For a fixed cathode potential, the current recorded increases with higher background gas pressures. This can be clearly seen in both Fig. 19 and Fig. 20. Now for grid 1 and grid 2, the current values are almost identical with a maximum difference of 2 mA observed at higher background pressures, as seen in Fig. 19. Lastly, the change in current recorded with background gas pressure is noted to be gradual, without any abrupt jump in current.

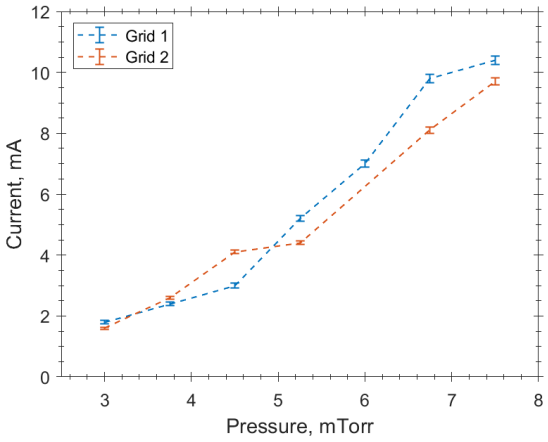

Fig. 19 Discharge characteristics for grid 1 and grid 2 at cathode potential = -3 kV.

Interestingly, it is observed in Fig. 20 that the discharge current (for fixed pressure and cathode potential) recorded when operating with grid 4 is more than twice the current values noted when operating with grid 3. The only difference in these two grids is the area of the exit hole through which the plasma beam comes out.

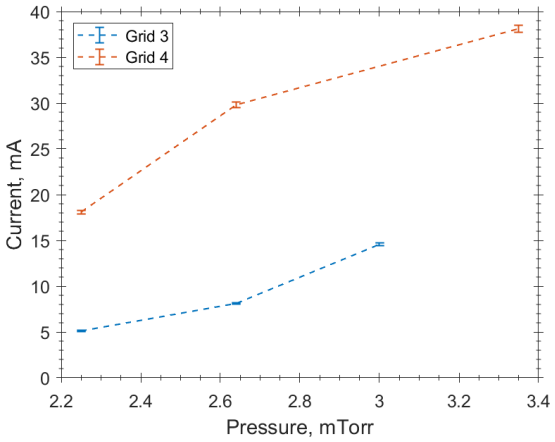

Fig. 20 Discharge characteristics for grid 3 and grid 4 at cathode potential = -3.75 kV.

2. Intensity Analysis

Figure 21 and Fig. 22 show the effect of increasing background pressure, keeping cathode potential constant, for all the four grids. It is observed that the overall light intensity of the system increases with an increase in background gas pressure. However, the visibility of ion microchannels goes down with the increasing background pressure, making the inter-electrode region look more uniform with regard to light intensity. It is also observed that the diameter of the central plasma core (high intensity hotspot) is bigger for higher background gas pressures. This can be seen when noticing the changes between Fig. 21(a) and Fig. 21(b), Fig. 21(c) and Fig. 21(d), Fig. 22(b) and Fig. 22(a), Fig. 22(c) and Fig. 22(d).

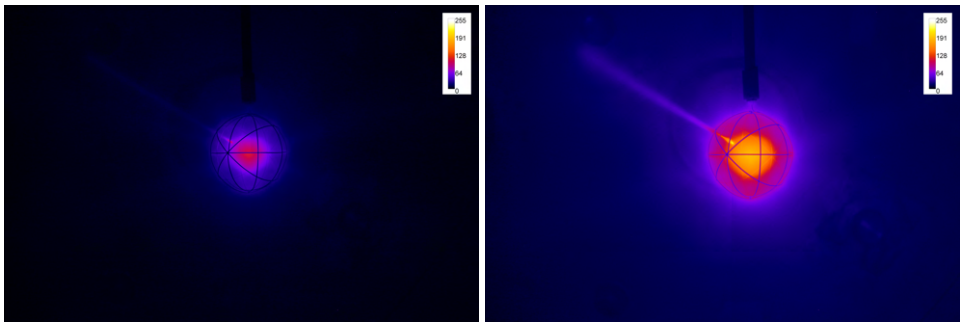

(a) Grid 1, pressure = 5.25 mTorr

(b) Grid 1, pressure = 7.5 mTorr

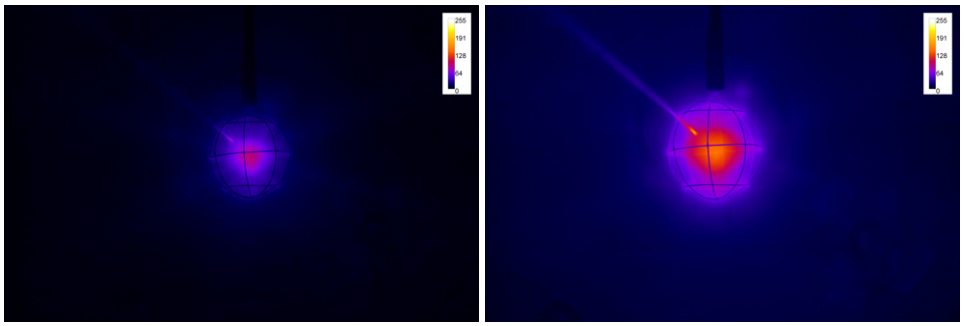

(c) Grid 2, pressure = 5.25 mTorr

(d) Grid 2, pressure = 7.5 mTorr

Fig. 21 IEC operating at cathode potential = -3 kV.

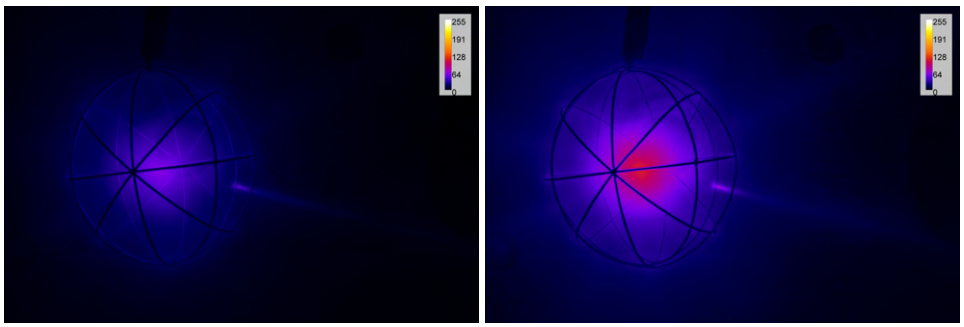

(a) Grid 3, pressure = 2.25 mTorr

(b) Grid 4, pressure = 3 mTorr

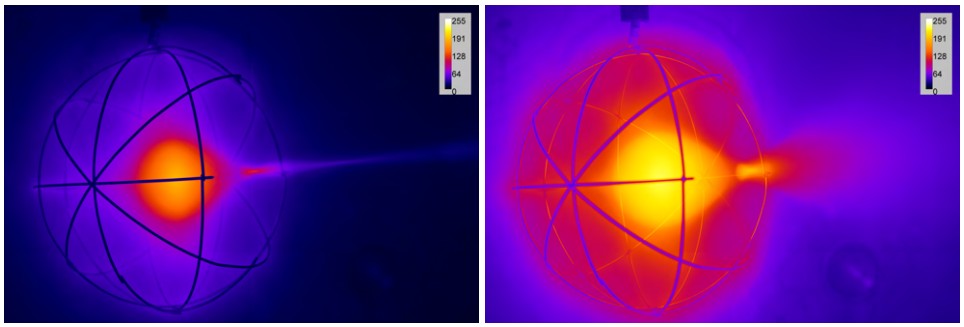

(c) Grid 3, pressure = 2.25 mTorr

(d) Grid 4, pressure = 3.35 mTorr

Fig. 22 IEC operating at cathode potential = -3.75 kV.

E. Cathode Potential

This section describes the changes in discharge characteristics and visual plasma structure when varying the applied cathode potential, keeping the background gas pressure constant.

1. Discharge Characteristics

Figure 23 shows the increase in current with increasing negative cathode potential, for all four grids used. Figure 23(a), shows operational points at a background pressure of 2 mTorr, at which none of the grids undergo abrupt changes in current. On the other hand, Fig. 23(b) shows the operational points at background gas pressure of 6.75 mTorr, at which three out of four grids have an abrupt, near vertical, increase in discharge current. In both the figures it is observed that the smaller grids have lower values of measured currents when compared to the larger grids, before any abrupt increase in current is encountered. Additionally, between the larger grids, grid 4 with larger opening area draws higher currents. However, as observed in Fig. 23(b), this trend is reversed for the grid 3 and grid 4 after passing through the abrupt increase in current. Lastly, the slope of the discharge curves is almost the same for all the four grids at the same background gas pressure.

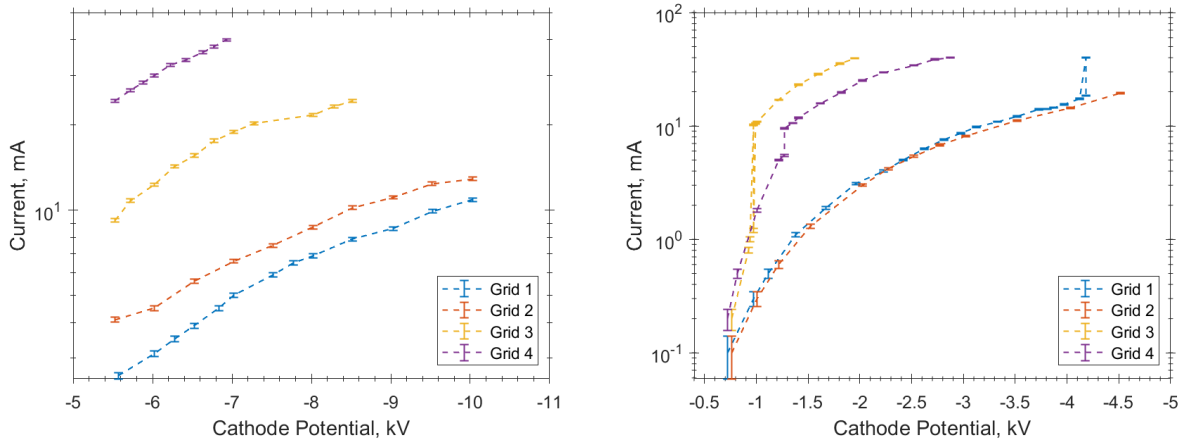

(a) Background gas pressure = 2 mTorr.

(b) Background gas pressure = 6.75 mTorr.

Fig. 23 Discharge characteristics at constant pressure.

2. Intensity Analysis

An increase in the overall light intensity of the images is observed at higher negative values of cathode potential. In Fig. 24, the size of the core region remains almost the same with the increase in the negative value of the cathode potential. However, the light intensity of the core increases, along with the visible length of the the ion microchannels, when the cathode potential is made more negative keeping the background gas pressure constant.

Similarly for grid 3 and grid 4 the light intensity of the overall device increases for higher negative cathode potential, keeping the background gas pressure fixed. This can be seen in Fig. 25. Likewise for a particular grid operation at constant background pressure, the size of the core remains fixed with the change in cathode potential. Additionally, the light intensity structure of the plasma beam diffuses more at higher values of negative cathode potential. Lastly, it is also noted that the peak light intensity, observed at the base of the plasma beam (detached from the core), goes up when the cathode potential is made more negative.

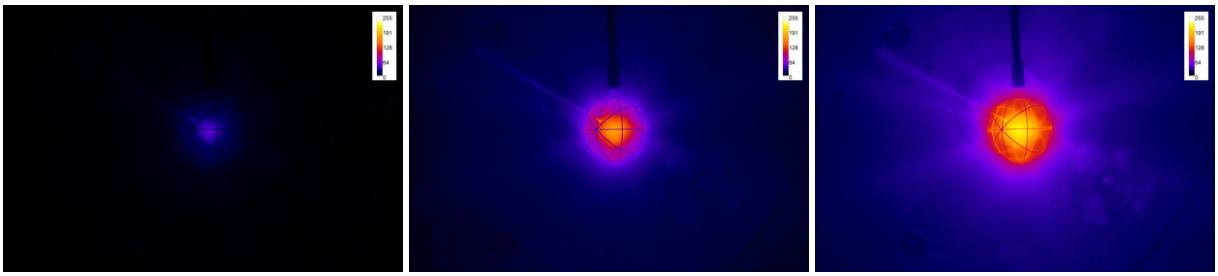

(a) Grid 1, cathode potential = -2 kV. (b) Grid 1, cathode potential = -4 kV. (c) Grid 1, cathode potential = -5 kV.

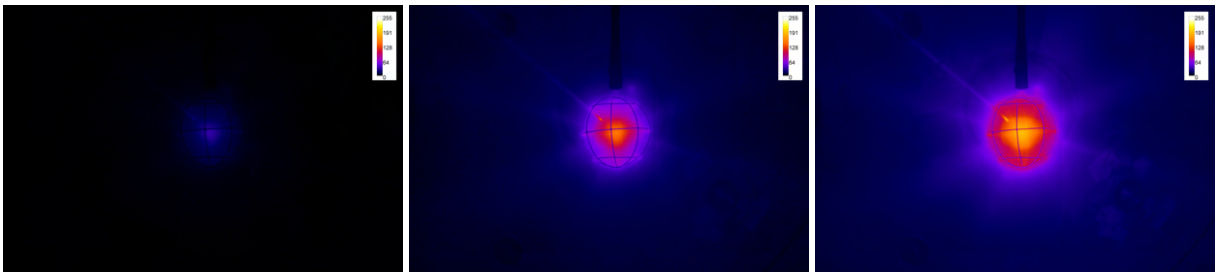

(d) Grid 2, cathode potential = -2 kV. (e) Grid 2, cathode potential = -4 kV. (f) Grid 2, cathode potential = -5 kV.

Fig. 24 IEC device operating at pressure = 5.25 mTorr.

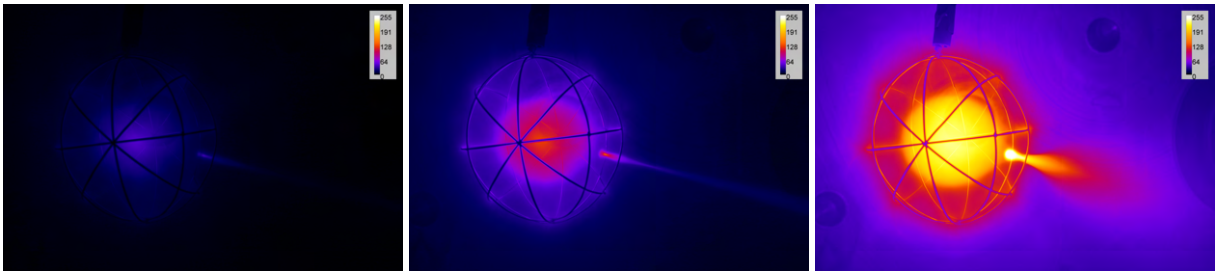

(a) Grid 3, cathode potential = -2.125 kV. (b) Grid 3, cathode potential = -2.975 kV. (c) Grid 3, cathode potential = -3.15 kV.

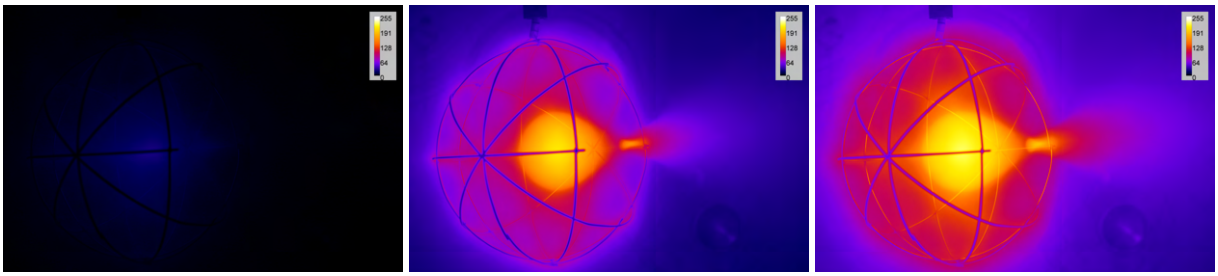

(d) Grid 4, cathode potential = -2.125 kV. (e) Grid 4, cathode potential = -2.975 kV. (f) Grid 4, cathode potential = -3.15 kV.

Fig. 25 IEC device operating at pressure = 3.35 mTorr.

F. Current Density

Preliminary Faraday probe measurements were conducted to identify the probe voltage bias range for a Faraday cup and Langmuir probe being designed for future experiments. Initially, the probe bias was swept from −1000 V to +1000 V. However, interference with the discharge plasma was noted due to the limitations on the sweeping frequency of the acquisition setup. Finally, a source meter was used to conduct the qualitative analysis for implementing future probes.

Due to the voltage range of the source meter only being from −20 V to +20 V, the probe did not reach either the electron or ion saturation region. But, current density for grounded probe and qualitative change in collected current vs. probe voltage was recorded. Grid 3 and grid 4 were used during these experiments at the background gas pressures depicted in Fig. 26.

Comparing Fig. 26(a) with Fig. 26(b), it is observed that the grid with larger opening (grid 4) had plasma current density at least an order of magnitude higher than the current density recorded with grid 3. Now for both the grids, the plasma current density increased with the increase in negative cathode potential. The increase in current density recorded was gradual, until an abrupt increase in current was observed for specific background pressure cases. For instance with grid 3, shown in Fig. 26(a), the near vertical increase in current density is observed for 3.35 mTorr and 6.75 mTorr background gas pressure. Similarly, for grid 4, the abrupt current density increase is observed for 3 mTorr background gas pressure. Incidentally, making cathode more negative after these points resulted in the the change from "jet" mode to "spray" mode (explained more in the Discussion section). Following the abrupt current density increase, the curve returned to the gradual slope that continued increasing with the higher value of negative cathode potential.

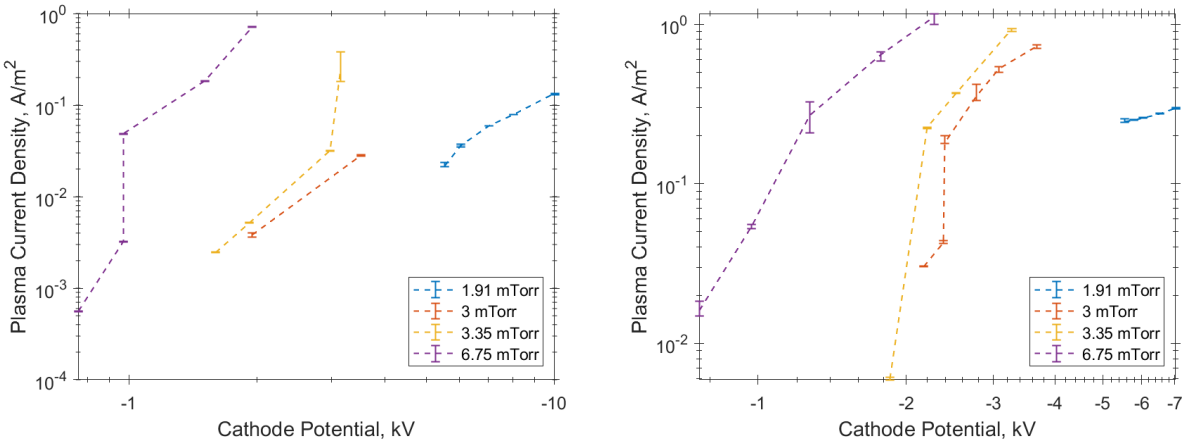

(a) Grid 3.

(b) Gird 4.

Fig. 26 Plasma current density measured with grounded Faraday probe.

V. Discussion

Until now, the results obtained were used to select an optimum grid design and dimensions, which will allow for the qualitative study of the "jet" mode inside an IEC device. It was found that grid 3 offered a more stable operation without grid overheating. The current section focuses primarily on the effects of independently changing the background gas pressure and cathode potential on the discharge characteristics and light intensity of the plasma generated, by using grid 3 with the IEC device.

A. Discharge Characteristics

Figure 27 shows a discharge characteristic plot expected for an IEC device, operating at three different background gas pressures. Firstly it is noted that higher negative voltages can be reached, without reaching the power supply current limit, by operating at lower background gas pressures. This is because at higher background pressures, more neutrals are present throughout the system and thus inter-particle collision cross-sections are larger. These neutrals, along with other charged species, undergo collisions with the energized charged particles and lead to higher plasma densities throughout the system [19, 20]. Secondly it is observed that with increasing negative cathode potential, at a fixed background pressure, the discharge current increases until the current limit of the power supply is reached. This increase in the discharge current with the changing cathode potential can take the following three distinct shapes based on the background pressure.

First, at relatively higher pressure, shown by the 5.25 mTorr IV curve in Fig. 27, an unstable region of abrupt oscillations in discharge current between a lower limit and upper limit are observed. This unstable region marks voltage

range of "jet" to "spray" transition. The device repeatedly transitions back and forth between the "jet" and the "spray" mode, oscillating at a constant frequency. As the voltage is made slightly more negative, the frequency of oscillation increases and the magnitude of current jump also increases. By increasing the cathode potential even more, the device jumps to "spray" mode and operates at considerably higher discharge currents than the "jet" mode. Upon making the cathode potential more negative after the stable "spray" mode is achieved, the discharge current continues to increase when making the cathode potential more negative. However, the slope of the IV curve is greater than the one recorded during the operation in "jet" mode. When the pressure is reduced and the experiment is repeated, it is seen that "jet" mode operates for a longer range of voltages, before abruptly changing into "spray" mode, without undergoing through the unstable transition region. This is shown by the 3.35 mTorr IV curve in Fig. 27. Lastly, the IV curve at 2.64 mTorr in Fig. 27 depicts the low pressure case where only "jet" mode is observed. It can be inferred from the discharge characteristics that the "spray" mode is more easily achieved at higher pressures, while the "jet" mode is more prevalent at lower pressures. More importantly, the "spray" mode always follows the "jet" mode.

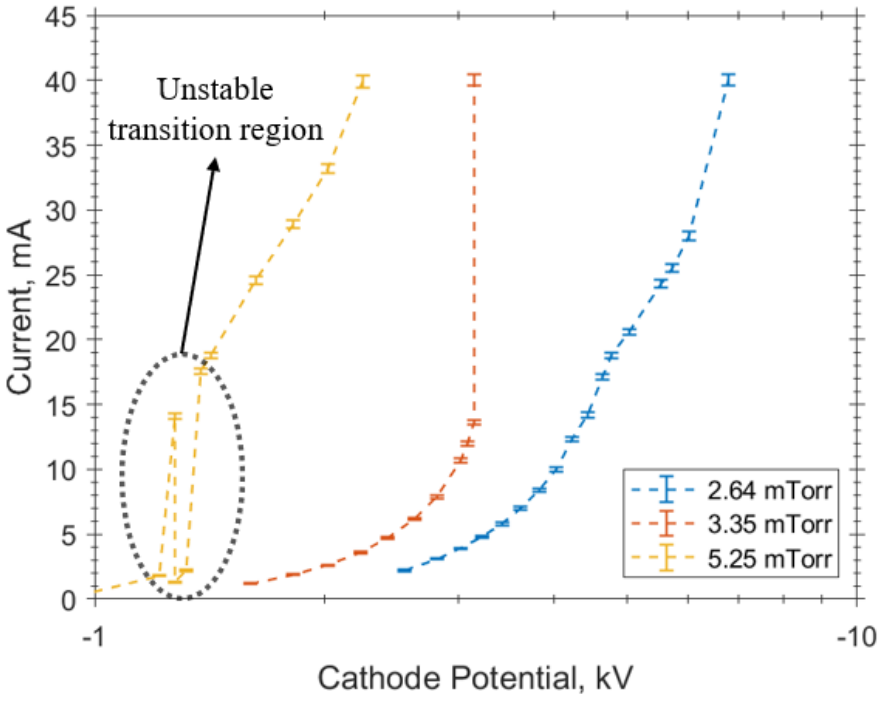

Fig. 27 Discharge characteristics for IEC operating with Grid 3.

B. Intensity Analysis

Figure 28 shows the evolution of the plasma structure in a low pressure discharge that only allows "jet" mode. It can be seen that a diamond-like structure is present near the base of the "jet", which gets brighter and sharper as the cathode potential is made more negative. The highest intensity point remains at the vertex of the diamond closer to the core. Additionally, the plasma beam in the "jet" seems to remain collimated and the tight beam structure is maintained until it reaches the anode. Contrary to the "jet", the "spray" structure is more diffuse and blends in with the inter-electrode plasma soon after leaving the cathode opening. This structure can be seen in Fig. 29. The base of the "spray", similar to the "jet", remains the highest light intensity point in the images captured. However, as opposed to the sharp diamond-like structure observed in the "jet" mode, the base of the "spray" is rounded near the core and cylindrical thereafter.

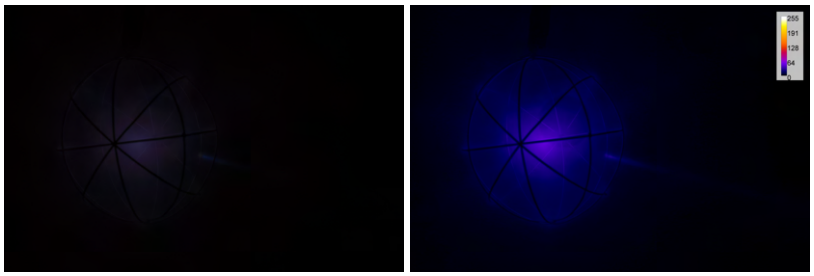

(a) Cathode potential = -2.77 kV. (b) Cathode potential = -2.77 kV.

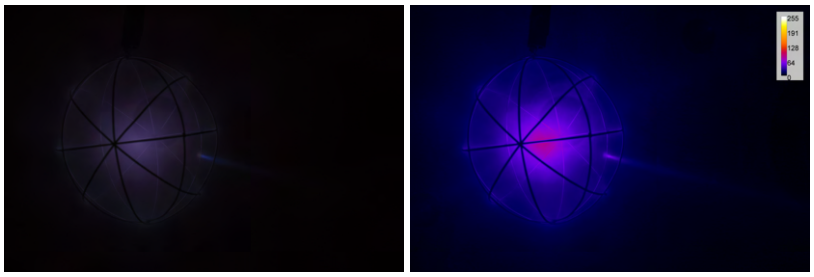

(c) Cathode potential = -3.33 kV. (d) Cathode potential = -3.33 kV.

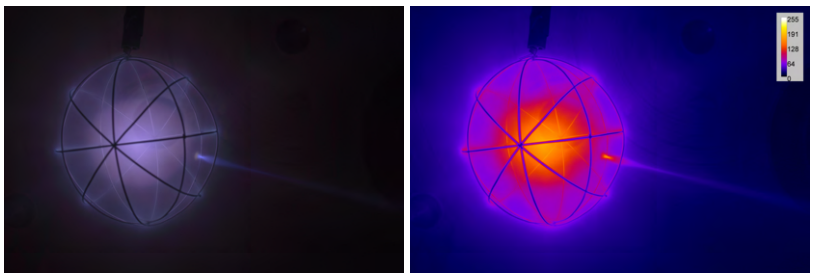

(e) Cathode potential = -4.76 kV. (f) Cathode potential = -4.76 kV.

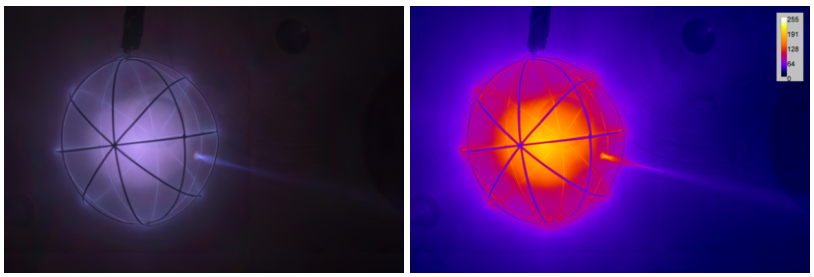

(g) Cathode potential = -5.53 kV. (h) Cathode potential = -5.53 kV.

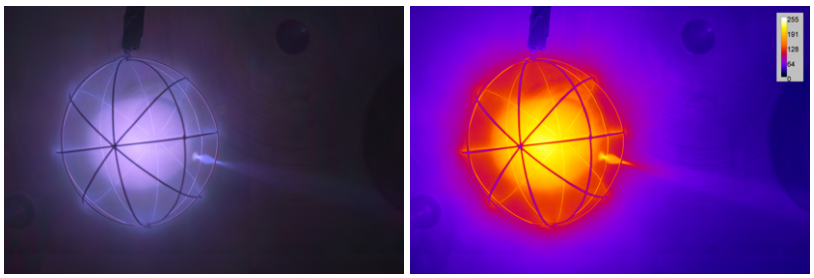

(i) Cathode potential = -6.78 kV. (j) Cathode potential = -6.78 kV.

Fig. 28 Image (left) and intensity spectrum (right) of grid 3 discharge operating at 2.64 mTorr.

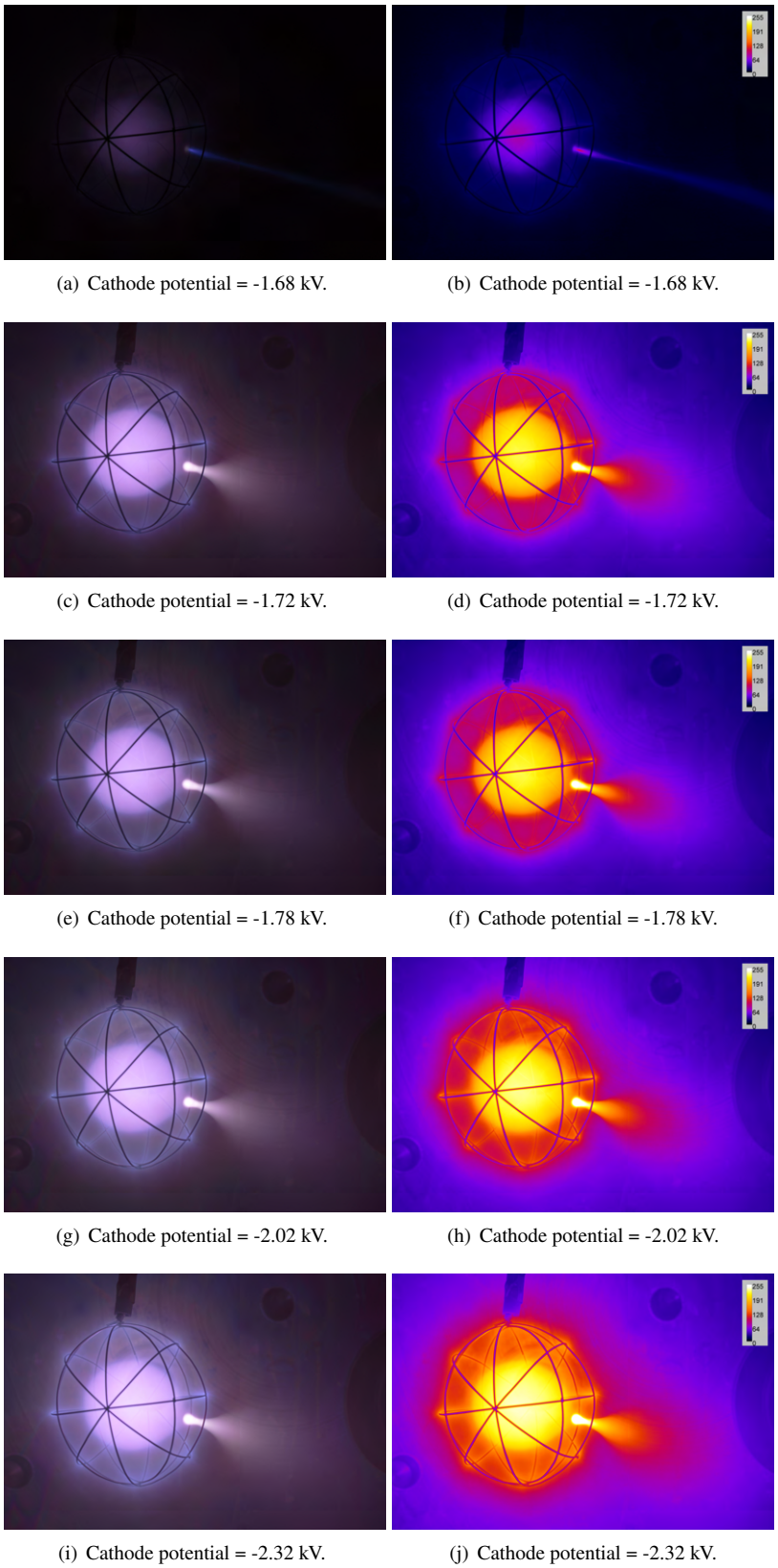

(a) Cathode potential = -1.68 kV. (b) Cathode potential = -1.68 kV.

(c) Cathode potential = -1.72 kV. (d) Cathode potential = -1.72 kV.

(e) Cathode potential = -1.78 kV. (f) Cathode potential = -1.78 kV.

(g) Cathode potential = -2.02 kV. (h) Cathode potential = -2.02 kV.

(i) Cathode potential = -2.32 kV. (j) Cathode potential = -2.32 kV.

Fig. 29 Image (left) and intensity spectrum (right) of grid 3 discharge operating at 4.5 mTorr.

C. Current Density

Figure 30 depicts a characteristic plasma current density plot for IEC discharge, measured by a Faraday probe placed away from the "jet" or "spray". Due to power limitations of the acquisition device, the probe was not able to reach either of the electron saturation and the ion saturation regime. However, certain qualitative relations could be deduced from the data collected. Firstly, both the "jet" and the "spray" mode have similar shape of the IV curve. However, the current density measured, and its change with respect to applied probe voltage, is orders of magnitude higher in the "spray" mode. Secondly, the magnitude of current drawn increases with an increase in the magnitude of negative cathode potential. Lastly, at pressures where both "jet" mode and "spray" mode exist, the curve that peaks faster can be used to identify the "spray" mode operation for discharge cases where the visible plasma is much more diffuse, as observed in the high pressure cases of "spray" mode with grid 4 (Fig. 25(f)).

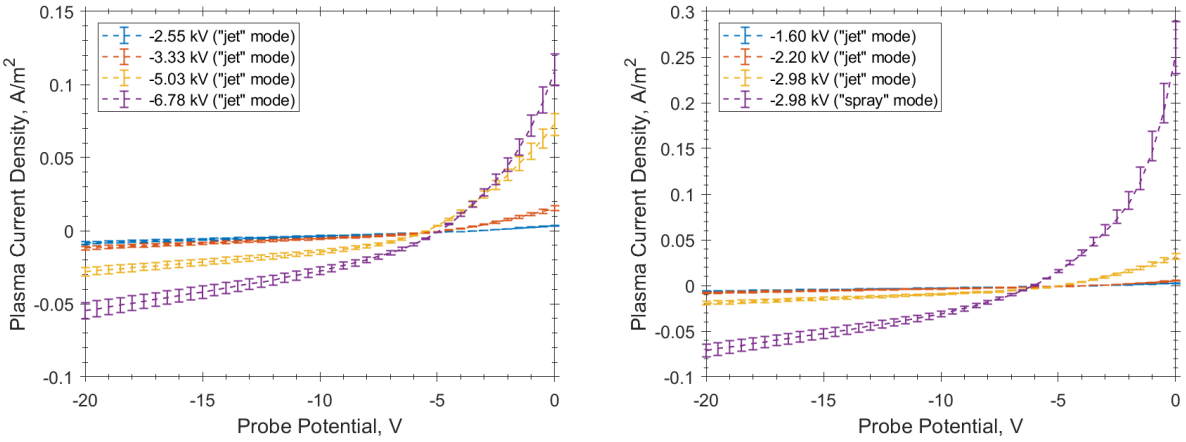

(a) Pressure = 2.64 mTorr.

(b) Pressure = 3.35 mTorr.

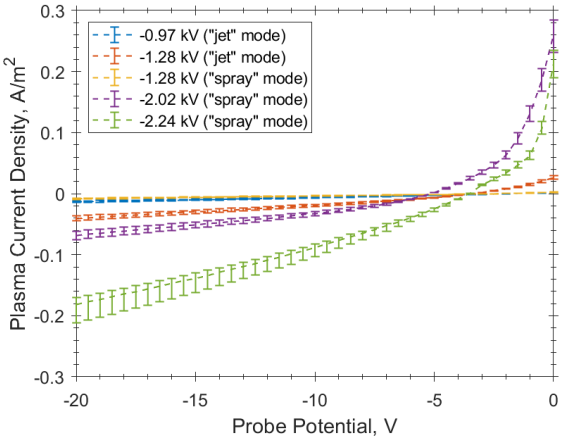

(c) Pressure = 5.25 mTorr.

Fig. 30 Plasma current density vs probe voltage for grid 3.

VI. Conclusion

For an asymmetric cathode grid, background gas pressure and applied cathode potential decide the mode of operation of the IEC system. While the background gas pressure had a a major effect on the mode of operation, the cathode potential impacted the visible plasma structure to a greater extent. The grid with the globe design sustained the "jet" mode for longer operating range, when compared to the geodesic grid design. The grid diameter directly impacted the discharge current and the scale of the visible plasma structure inside the IEC system. Additionally, smaller grids

were able to sustain the "jet" mode for longer range of background gas pressures. A "jet" mode was favored for lower pressures till a threshold pressure, dependent on grid dimensions, was reached. For larger diameter grids, the threshold pressure is higher (nearly 6 mTorr) as opposed to the lower threshold value (nearly 3.35 mTorr) for smaller diameter grids. Beyond the threshold background gas pressure, the "jet" mode transitions to the "spray" mode with increasing negative cathode potential. Depending on the background gas pressure, the "jet" to "spray" transition can be abrupt, or can pass through a region of unstable oscillations till a the cathode potential is made more negative, to reach the "spray" mode. The unstable transition region is observed for pressures above 7.5 mTorr for most of the grids tested. Finally, a fundamental difference between the "jet" and the "spray" mode was identified using the measured plasma current densities and discharge characteristics. For "jet" mode, the current density peaked at 0.2 $A.m^{-2}$ for low pressure and high cathode potential (more negative) operation points. However, the "spray" mode operation involved plasma current densities measured from 0.2 $A.m^{-2}$ to 1.2 $A.m^{-2}$, higher values for higher pressures or more negative cathode potential.

Acknowledgments

Support from the NPL Associates INC is gratefully acknowledged.

References

[1] Miley, G. H., and Murali, S. K., *Inertial Electrostatic Confinement (IEC) Fusion: Fundamentals and Applications*, Springer New York, 2014. https://doi.org/10.1007/978-1-4614-9338-9.

[2] Wu, L., and Miley, G. H., "IEC-Based Neutron Generator for Security Inspection System," *10th International Conference on Nuclear Engineering*, American Society of Mechanical Engineers Digital Collection, 2009, pp. 921–926. https://doi.org/10.1115/ICONE10-22696.

[3] Miley, G. H., Bromley, B. P., and Gu, Y., "A novel IEC propulsion unit for satellite applications," *AIP Conference Proceedings*, Vol. 361, AIP, 1996, pp. 1435–1440. https://doi.org/10.1063/1.49918, URL https://pubs.aip.org/aip/acp/article/361/1/1435-1440/609108, ISSN: 0094243X.

[4] Egle, B. J., Santarius, J. F., and Kulcinski, G. L., "Comparison of Spherical and Cylindrical Cathode Geometries in Inertial Electrostatic Confinement Devices," *Fusion Science and Technology*, Vol. 52, No. 4, 2007, pp. 1110–1113. https://doi.org/10.13182/FST07-A1646.

[5] Ahern, D., "Investigation of a Space Propulsion Concept Using Inertial Electrostatic Confinement," Ph.D. thesis, Dept. of Aerospace, University of Illinois Urbana-Champaign, Urbana, IL, 2018.

[6] Miley, G. H., Javedani, J., Yamamoto, Y., Nebel, R., Nadler, J., Gu, Y., Satsangi, A., and Heck, P., "Inertial-Electrostatic Confinement Neutron/Proton Source," *AIP Conference Proceedings*, Vol. 299, No. 1, 1994, pp. 675–689. https://doi.org/10.1063/1.2949222, AIP Conference Proceedings.

[7] Miley, G., Gu, Y., DeMora, J., Stubbers, R., Hochberg, T., Nadler, J., and Anderl, R., "Discharge characteristics of the spherical inertial electrostatic confinement (IEC) device," *IEEE Transactions on Plasma Science*, Vol. 25, No. 4, 1997, pp. 733–739. https://doi.org/10.1109/27.640696.

[8] Puri, R., Miley, G. H., Rovey, J. L., Ziehm, E. P., Patino, R., and Najam, R. S., "Characterizing Plasma Jet of HIIPER," *ASCEND 2022*, American Institute of Aeronautics and Astronautics, 2022. https://doi.org/10.2514/6.2022-4272.

[9] Puri, R., Miley, G. H., Ziehm, E. P., Patino, R., and Najam, R. S., "Helicon Injected Inertial Plasma Electrostatic Rocket," *Nuclear Technology*, Vol. 208, 2022, pp. S85–S95. https://doi.org/10.1080/00295450.2022.2055702.

[10] Hirsch, R. L., "Inertial-Electrostatic Confinement of Ionized Fusion Gases," *Journal of Applied Physics*, Vol. 38, No. 11, 1967, pp. 4522–4534. https://doi.org/10.1063/1.1709162.

[11] Krishnamurthy, A., "Development and Characterization of an Inertial Electrostatic Confinement Thruster," Ph.D. thesis, Dept. of Aerospace, University of Illinois Urbana-Champaign, Urbana, IL, 2012.

[12] Syring, C., and Herdrich, G., "Discharge and Operational Conditions of an Inertial Electrostatic Confinement Device," *49th AIAA/ASME/SAE/ASEE Joint Propulsion Conference*, 2023. https://doi.org/10.2514/6.2013-4025.

[13] Chan, Y.-A., and Herdrich, G., "Breakthrough of Inertial Electrostatic Confinement Concept for Advanced Space Propulsion," *International Astronautical Congress*, 2018.

[14] Mazouffre, S., Largeau, G., Garrigues, L., Boniface, C., and Dannenmayer, K., "Evaluation of various probe designs for measuring the ion current density in a Hall thruster plume." *35th International Electric Propulsion Conference*, 2017.

[15] Brown, D. L., Walker, M. L. R., Szabo, J., Huang, W., and Foster, J. E., "Recommended Practice for Use of Faraday Probes in Electric Propulsion Testing," *Journal of Propulsion and Power*, Vol. 33, No. 3, 2017, pp. 582–613. https://doi.org/10.2514/1.B35696.

[16] Schneider, C. A., Rasband, W. S., and Eliceiri, K. W., "NIH Image to ImageJ: 25 years of image analysis," *Nature Methods*, 2012, pp. 671–675. https://doi.org/https://doi.org/10.1038/nmeth.2089.

[17] Syring, C., and Herdrich, G. H., "Experimental Discharge Characterization and Scaling of IEC Plasma Devices," *33rd International Electric Propulsion Conference*, 2013.

[18] Chan, Y.-A., and Herdrich, G., "Jet extraction and characterization in an inertial electrostatic confinement device," *Vacuum*, Vol. 167, 2019, pp. 482–489. https://doi.org/10.1016/j.vacuum.2018.07.053.

[19] Miley, G. H., Puri, R., and Cai, Q., "Study of the Helicon Injected Inertial Plasma Electrostatic Rocket (HIIPER) Integrated with a Magnetic Nozzle," *ASCEND 2020*, American Institute of Aeronautics and Astronautics, 2020. https://doi.org/10.2514/6.2020-4083.

[20] Puri, R., Miley, G. H., Ziehm, E. P., Patino, R., and Najam, R. S., "Performance Analysis of HIIPER MPD Thruster," *AIAA Propulsion and Energy 2021 Forum*, American Institute of Aeronautics and Astronautics, 2021. https://doi.org/10.2514/6.2021-3402.